

Predicting drag on rough surfaces by transfer learning of empirical correlations

Sangseung Lee¹†, Jiasheng Yang², Pourya Forooghi³, Alexander Stroh², and Shervin Bagheri¹‡

¹Department of Engineering Mechanics, FLOW Centre, KTH, Stockholm SE-100 44, Sweden

²Institute of Fluid Mechanics, Karlsruhe Institute of Technology, Karlsruhe 76131, Germany

³Department of Mechanical and Production Engineering, Aarhus University, 8000, Aarhus C, Denmark

(Received xx; revised xx; accepted xx)

Recent developments in neural networks have shown the potential of estimating drag on irregular rough surfaces. Nevertheless, the difficulty of obtaining a large high-fidelity dataset to train neural networks is deterring their use in practical applications. In this study, we propose a transfer learning framework to model the drag on irregular rough surfaces even with a limited amount of direct numerical simulations. We show that transfer learning of empirical correlations, reported in the literature, can significantly improve the generalization ability of neural networks for drag prediction. The developed framework can be applied to applications where acquiring a large dataset is difficult, but empirical correlations have been reported.

Key words:

1. Introduction

Nearly all surfaces in fluid-related industries are rough at their operating Reynolds numbers. These rough surfaces easily alter the aero- or hydrodynamic properties of a fluid system and induce unfavorable consequences; for instance, reduced stability of aircraft, increased fuel consumption of cargo ships, and reduced energy harvesting capacity of wind turbines (Gent *et al.* 2000; Schultz *et al.* 2011; Dalili *et al.* 2009). Therefore, it is crucial to restore or replace surfaces that have degraded past a critical level. This requires monitoring roughness on industrial surfaces and efficiently predicting their effect on the flow.

One of the most representative effects of surface roughness on flow is the increased drag. This additional drag is generally expressed by the Hama roughness function (Hama 1954) or the equivalent sand-grain height. The Hama roughness function is the downward shift of the mean velocity profile induced by roughness. The equivalent sand-grain height is the roughness height from the Moody diagram (Moody 1944) that would cause the same drag as the rough surface of interest. It is worth noting that to calculate the equivalent sand-grain height, the Hama roughness function in the fully-rough regime – where the skin-friction coefficient is independent of Reynolds number – needs to be determined.

To accurately determine the Hama roughness function of irregular surfaces, numerical simulations with fully resolved rough structures or experiments are needed. However, neither simulations nor experiments are cost-efficient, hence not feasible for practical purposes. To alleviate the high

† Email address for correspondence: sanlee@mech.kth.se

‡ Email address for correspondence: shervin@mech.kth.se

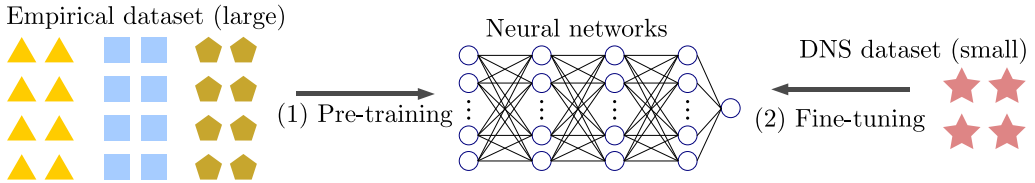


FIGURE 1. Overview of the transfer learning framework.

costs, researchers have found empirical correlations between rough surface statistics and their contribution to drag (Chan *et al.* 2015; Forooghi *et al.* 2017; Flack & Schultz 2010; Flack *et al.* 2020). However, no universal model has emerged that is able to accurately predict the drag from a sufficiently wide range of roughness. This is mainly attributed to the high-dimensional feature space of irregular rough structures (Chung *et al.* 2021).

Neural networks are known to be capable of extracting patterns in high-dimensional spaces, and therefore have been successfully used in various studies using fluid flow data (Lee & You 2019; Kim & Lee 2020; Fukami *et al.* 2021). Jouybari *et al.* (2021) developed a multilayer perceptron (MLP) type neural network to find a mapping of 17 different rough surface statistics to equivalent sand-grain height. They reported a state-of-the-art performance in predicting equivalent sand-grain heights from rough surface statistics. A total of 45 data samples, obtained from direct numerical simulations (DNS) and experiments, were used for training and validating their neural network. Having a large number of data samples to train a neural network is invariably advantageous; nonetheless, constructing a fluid database that is sufficiently large to train a network from scratch imposes significant computational or experimental cost and is oftentimes considered impractical. Therefore, for the practical usage of neural networks in fluid-related applications, a framework that allows neural networks to learn a generalized mapping from a limited number of data samples is needed.

In this study, we propose a transfer learning framework to improve the generalization ability of neural networks for predicting the drag on rough surfaces when only a limited number of high-fidelity data samples are available. Transfer learning is a method that improves learning performance by adapting knowledge learned from one domain to another (Pan & Yang 2009; Chakraborty 2021). We show that adapting knowledge of empirical correlations to the domain of high-fidelity physics can significantly improve the learning performance.

2. Transfer learning framework

The developed transfer learning framework is composed of two steps: (1) pre-training step and (2) fine-tuning step (figure 1). In the pre-training step, neural networks were trained to learn an ‘approximate’ knowledge of the mapping of surface statistics to the Hama roughness function from a large dataset of multiple empirical correlations. In the fine-tuning step, neural networks were tuned to learn high-fidelity physics from a small DNS dataset by adapting their pre-trained ‘approximate’ knowledge to the domain of real physics. In section 3, we show that transfer learning of empirical correlations improves the generalization ability of neural networks when learning the drag of rough surfaces from a small amount of data. First however, we explain the details of the neural networks and pre-training and fine-tuning steps.

2.1. Neural network

We used a variation of the MLP type neural network architecture developed by Jouybari *et al.* (2021). The input of the employed network is a set of 17 different rough surface statistics calculated from the surface topography of interest. Let x , y , and z be the streamwise, wall-normal and spanwise directions, $k(x, z)$ the roughness height distribution and A_r the total roughness area.

$$\begin{aligned}
 I_1 &= k_{rms}/Ra & I_2 &= Sk = \frac{1}{A_t} \int_{x,z} (k - k_{avg})^3 dA / k_{rms}^3 \\
 I_3 &= kur = \frac{1}{A_t} \int_{x,z} (k - k_{avg})^4 dA / k_{rms}^4 & I_4 &= ES_x = \frac{1}{A_t} \int_{x,z} \left| \frac{\partial k}{\partial x} \right| dA \\
 I_5 &= ES_z = \frac{1}{A_t} \int_{x,z} \left| \frac{\partial k}{\partial z} \right| dA & I_6 &= por = \frac{1}{A_t k_c} \int_0^{k_c} A_f dy \\
 I_7 &= inc_x = \tan^{-1} \left\{ \frac{1}{2} Sk \left(\frac{\partial k}{\partial x} \right) \right\} & I_8 &= inc_z = \tan^{-1} \left\{ \frac{1}{2} Sk \left(\frac{\partial k}{\partial z} \right) \right\} \\
 I_9 &= I_4 I_5 & I_{10} &= I_4 I_2 \\
 I_{11} &= I_4 I_3 & I_{12} &= I_5 I_2 \\
 I_{13} &= I_5 I_3 & I_{14} &= I_2 I_3 \\
 I_{15} &= I_4 I_4 & I_{16} &= I_5 I_5 \\
 I_{17} &= I_2 I_2
 \end{aligned}$$

TABLE 1. Statistical input parameters of the employed neural network.

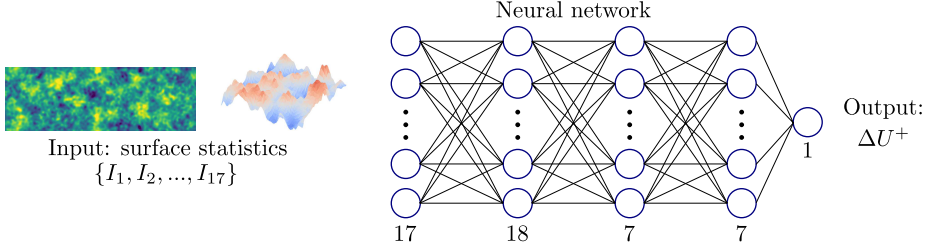


FIGURE 2. Architecture of the used neural network.

Then, one may define the following measures of an irregular rough surface: average roughness height $k_{avg} = \int_{x,z} k dA / A_t$, average height deviation $Ra = \int_{x,z} (|k - k_{avg}|) dA / A_t$, root-mean-squared roughness height $k_{rms} = (\int_{x,z} (k - k_{avg})^2 dA / A_t)^{1/2}$, crest height k_c , and finally, fluid area at each wall-normal plane $A_f(y)$. From these quantities, the 17 statistical input parameters ($\{I_1, I_2, \dots, I_{17}\}$) can be calculated as listed in table 1. Here, Sk , kur , por , ES_x , ES_z , inc_x , and inc_z indicate skewness, kurtosis, porosity, and effective slopes and average inclinations in x and z directions, respectively. Before training, the parameters I_1 to I_{17} were normalized with the mean and standard deviation values calculated from the dataset of empirical correlations (see section 2.2 for the details of the empirical dataset).

Information of input parameters travels through three hidden layers with 18, 7, and 7 neurons, respectively (see figure 2). Leaky ReLU activations ($\max(0.01x, x)$) were applied after the hidden layers. The output of the employed neural network is a scalar value of the Hama roughness function ΔU^+ . The superscript $+$ indicates the normalization by the viscous scale $\delta_v = \nu / u_\tau$, where ν and u_τ are the kinematic viscosity and the friction velocity, respectively. In this study, the friction Reynolds number $Re_\tau = u_\tau H / \nu = 500$ was used, where H is the channel half-height. At the output layer, a Sigmoid activation function, $a / (1 + e^x)$, was applied to bound the prediction value ($a = 20$ in this study).

2.2. Pre-training step

In the pre-training step, neural networks were trained with a large dataset of empirical correlations between rough surface statistics and the Hama roughness function ΔU^+ . We used three correlations;

$$\Delta U^+ = 2.5 \log Ra^+ + 1.12 \log ES_x + 1.47; \quad (\text{EMP1})$$

$$\Delta U^+ = 2.5 \log [k_c^+ (0.67 Sk^2 + 0.93 Sk + 1.3) (1.07 (1 - e^{-3.5 ES_x}))] - 3.5; \quad (\text{EMP2})$$

and

$$\Delta U^+ = \begin{cases} 2.5 \log[2.48k_{rms}^+(1 + Sk)^{2.24}] - 3.5, & Sk > 0 \\ 2.5 \log[2.11k_{rms}^+] - 3.5, & Sk \approx 0, \\ 2.5 \log[2.73k_{rms}^+(2 + Sk)^{-0.45}] - 3.5, & Sk < 0. \end{cases} \quad (\text{EMP3})$$

Here, **EMP1** was proposed by Chan *et al.* (2015), **EMP2** by Forooghi *et al.* (2017) and **EMP3** by Flack & Schultz (2010); Flack *et al.* (2020).

Note that **EMP1** to **EMP3** were mainly developed in the fully rough regime. The friction Reynolds number ($Re_\tau = 500$) used in the current study may not be sufficient to render all of the generated surfaces fully rough. Nonetheless, these empirical models inherently contain an ‘approximate’ knowledge of the mapping of surface statistics to the Hama roughness function that will help the neural network to learn the real physics in the fine-tuning step.

A large dataset was constructed by randomly generating 10,000 irregular rough surfaces and calculating the associated Hama roughness function using **EMP1** to **EMP3**. The surfaces were constructed using the Fourier-filtering algorithm suggested by Jacobs *et al.* (2017). This algorithm generates surfaces by a superposition of waves, whose amplitudes are chosen randomly from a Gaussian distribution (see figure 3a for examples of the generated surfaces). For training and validating the neural network, 7,000 and 3,000 data samples were employed, respectively. Figure 3b shows the scatter plots of the Hama roughness functions, calculated by **EMP1** to **EMP3**, against k_{rms} , Sk , and ES_x from the 3,000 validation data samples. We observe different distributions, or knowledge, of the Hama roughness function from the different empirical models. The aim is to seed this diverse knowledge of empirical correlations in neural networks during the pre-training step.

Three neural networks with the same architecture and the same initial weights and biases were trained simultaneously to learn the different empirical models, **EMP1** to **EMP3**. Let NN^i be the neural network trained with the i -th empirical model, $W_{j,k}^i$ the weight matrix connecting the j -th and k -th layers of NN^i , N_w the total number of weights in NN^i , b_j^i the bias vector added in the j -th layer, ΔU_i^+ the Hama roughness function predicted by the i -th empirical model, and $\Delta \tilde{U}_i^+$ the Hama roughness function predicted by NN^i . The neural networks were trained to minimize a loss for pre-training:

$$L_p = \frac{1}{3} \sum_{i=1}^3 \left[\left(\Delta U_i^+ - \Delta \tilde{U}_i^+ \right)^2 + \sum_{j,k} \text{tr} \left\{ (W_{j,k}^i)^T (W_{j,k}^i) \right\} \right]. \quad (2.1)$$

The first term in the right-hand side is the mean-squared-error loss and the second is the weight regularization loss, also used in Jouybari *et al.* (2021). The sizes of the weight matrix $W_{j,k}^i$ and bias vector b_k^i are $n_j \times n_k$ and n_k , respectively, where n_j and n_k are the number of neurons on the j -th and k -th layers.

The weights and biases of the neural networks were updated in the direction of minimizing the pre-training loss L_p on the training data samples through the Adam optimizer (Kingma & Ba 2014). The pre-training loss L_p on the validation data samples was also evaluated each iteration of updates. Batch sizes of 16 and 32 were used for training and validating, respectively. To provide a wide distribution of data samples in the batches, i.e., preventing neural networks from learning biased data focused on average characteristics, we imposed batches to contain 50% of the data samples with ΔU^+ in the range 6 to 8, 25% of the data samples with ΔU^+ in the range 4 to 6, and the remaining 25% of the data samples with ΔU^+ in the range 8 to 10. After a sufficient amount of iterations for training and validating, the set of networks ($\{NN^1, NN^2, NN^3\}$) that produced the lowest pre-training loss on the validation data samples was chosen to be merged into a single pre-trained network NN^{pre} . The learned sets of weights and biases in the three neural networks, $\{W_{j,k}^1, W_{j,k}^2, W_{j,k}^3\}$ and $\{b_k^1, b_k^2, b_k^3\}$, were averaged into the weights and biases of $W_{j,k}^{pre}$ and

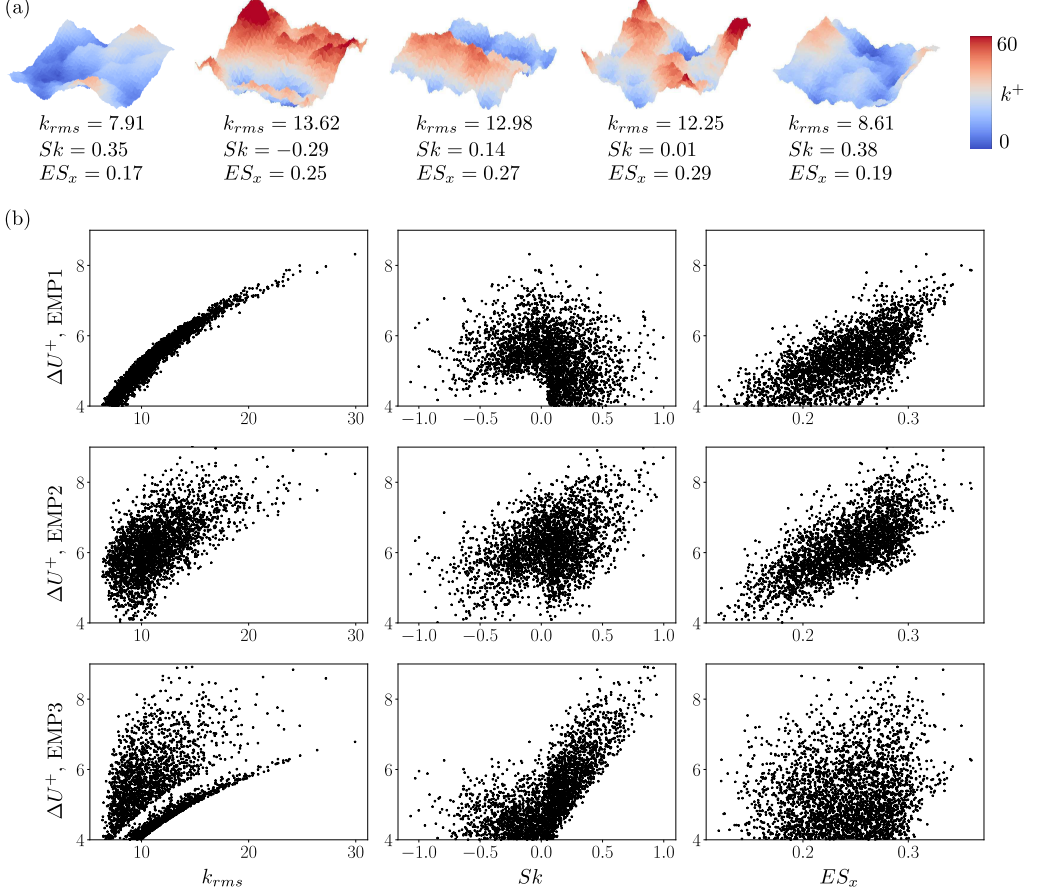


FIGURE 3. (a) Examples of patches of the generated surfaces in the empirical dataset. The size of the patches is $H \times H$ in the streamwise and spanwise directions. (b) Scatter plots of the Hama roughness functions (ΔU^+), calculated by **EMP1**, **EMP2**, and **EMP3**, against k_{rms} , Sk , and ES_x from the 3,000 validation data samples.

b_k^{pre} as $W_{j,k}^{pre} = \sum_{i=1}^3 W_{j,k}^i / 3$ and $b_k^{pre} = \sum_{i=1}^3 b_k^i / 3$. These pre-trained weights and biases were employed as the initial weights for the fine-tuning step (section 2.3) to transfer the knowledge of empirical correlations to the domain of high-fidelity physics.

2.3. Fine-tuning step

A total of 35 DNS of channel flow over rough surfaces at $Re_\tau \approx 500$, in the transitionally and fully rough regimes, were conducted to construct a high-fidelity dataset. The 35 rough surfaces were generated with randomly prescribed power spectra and height probability distributions following the generation method proposed by Pérez-Ràfols & Almqvist (2019) (see figure 4a for examples of the generated surfaces). It is worth noting that different surface generation methods were used to construct the DNS and empirical datasets (section 2.2). Indeed, in realistic situations, surfaces are likely to be inherently different with the generated surfaces for the empirical datasets.

Details of the methodology and validation of the conducted DNS are reported in the study of Yang *et al.* (2021). Here, we provide a brief overview. A pseudo-spectral incompressible Navier–Stokes solver, SIMSON (Chevalier *et al.* 2007) with an immersed boundary method (Goldstein *et al.* 1993), was employed for the channel simulations. Periodic

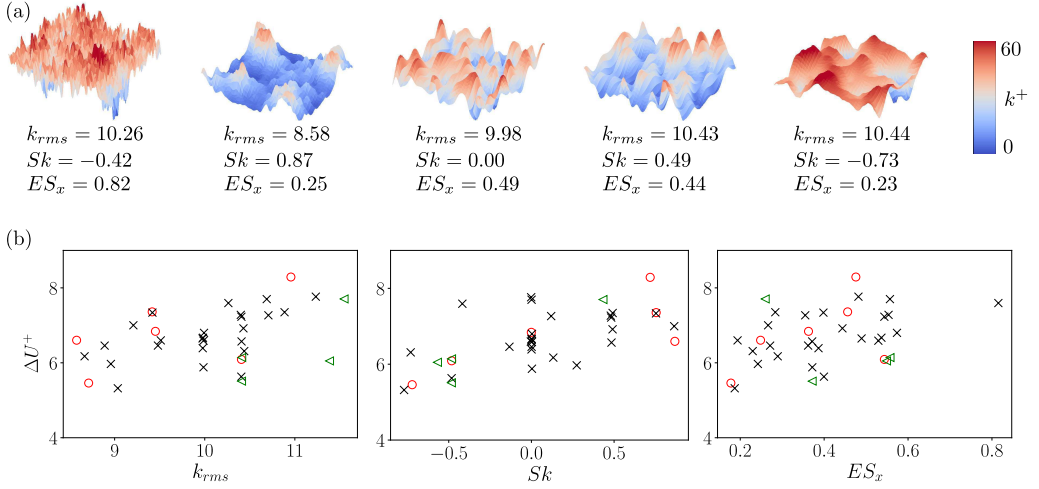


FIGURE 4. (a) Examples of patches of the generated surfaces in the DNS dataset. The size of the patches is $H \times H$ in the streamwise and spanwise directions. (b) Scatter plots of the calculated Hama roughness function (ΔU^+) against k_{rms} , Sk , and ES_x from the 35 DNS data samples. The markers \circ , \triangleleft , and \times indicate the training, validation, and test data samples, respectively. The plots were drawn from an example of a combination of training and validation data samples.

boundary conditions were used in the streamwise and spanwise directions. No-slip conditions were applied at the top and bottom planes of the channel. Roughness effects were added to both the top and bottom planes. A minimal channel approach was adopted to find a small computational domain size that can accurately reproduce the Hama roughness function calculated from a full channel simulation (Chung *et al.* 2015). For a given channel half height H , the domain and grid sizes for the full channel simulations were, respectively, $(8H \times 2H \times 4H)$ and $(900 \times 401 \times 480)$, in the streamwise, wall-normal, and spanwise directions. The smallest domain and grid sizes for the minimal channel simulations were $(2.0H \times 2H \times 0.4H)$ and $(256 \times 401 \times 48)$, respectively.

The scatter plots of the calculated Hama roughness function on the 35 data samples against surface statistics of k_{rms} , Sk , and ES_x are shown in figure 4b. The 35 data samples were split into 6, 4, and 25 data samples for training, validation, and test, respectively. It is worth noting that more than 70% of the data samples were used for testing, i.e., not used during the fine-tuning step, to fairly evaluate the generalization ability of the developed neural networks. The surface statistics and the Hama roughness function in the test dataset are distributed widely in the total dataset as shown by the \times markers in figure 4b.

To reduce the uncertainty arising from splitting a very small dataset into training and validation sets, we adopted an approach based on averaging many neural networks. More specifically, we employed 210 neural networks, $\{NN^1, NN^2, \dots, NN^{210}\}$, to learn from the 210 different combinations of 6 training and 4 validation data samples ($\binom{10}{6} = 10!/(6!4!) = 210$). The weights and biases of these 210 neural networks ($\{W_{j,k}^1, W_{j,k}^2, \dots, W_{j,k}^{210}\}$ and $\{b_k^1, b_k^2, \dots, b_k^{210}\}$) were initialized by the pre-trained weights and biases, $W_{j,k}^{pre}$ and b_k^{pre} . Similar to the pre-training step, the weights and biases of each neural network NN^i were updated by the Adam optimizer that minimizes a loss for fine tuning L_f^i ,

$$L_f^i = \left(\Delta U^+ - \Delta \tilde{U}_i^+ \right)^2 + \frac{1}{N_w} \sum_{j,k} \text{tr} \left\{ (W_{j,k}^i)^T (W_{j,k}^i) \right\}. \quad (2.2)$$

Here, ΔU^+ is the ground truth, and $\Delta \tilde{U}_i^+$ is the roughness function predicted by NN^i . After a

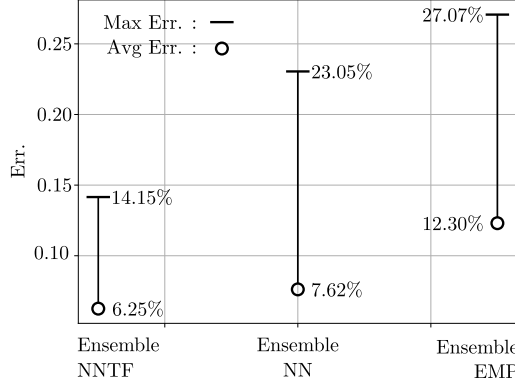


FIGURE 5. Average and maximum errors from the ensemble predictions performed by NNTF, NN, and EMP.

sufficient amount of updates, the networks with the smallest fine-tuning loss on the validation data samples were chosen to predict the roughness function ΔU^+ on test data (section 3).

3. Prediction results on test data

We compare the predicted Hama roughness functions on the 25 test data samples that were not included in the fine-tuning step. The roughness functions are calculated by the following prediction methods: (1) neural networks trained with transfer learning (NNTF), (2) neural networks trained without transfer learning (NN), and (3) empirical correlations (EMP). Neural networks in NN were trained without the pre-training step, i.e., the weights and biases of the networks were randomly initialized instead of being initialized by $W_{j,k}^{pre}$ and b_k^{pre} . Our focus here is on the comparison between NNTF and NN to demonstrate the effects of transfer learning. However, we also include EMP predictions in the comparison since these methods are widespread in the literature.

The performance of neural networks can vary greatly depending on the selection of data for training and validation. This is because it is generally hard to form a distribution covering the entire feature space from a limited number of data samples. By ensemble averaging the predictions from neural networks learned from different data combinations, we can partly alleviate this problem. The ensemble predictions from NNTF and NN are thus obtained by averaging the prediction values of the 210 neural networks as $\Delta \tilde{U}^+ = \sum_{i=1}^{210} \Delta \tilde{U}_i^+ / 210$. Similarly, we use ensemble predictions of the empirical models {EMP1, EMP2, EMP3} in EMP as $\Delta \tilde{U}^+ = \sum_{i=1}^3 \Delta \tilde{U}_{i,emp}^+ / 3$, where $\Delta \tilde{U}_{i,emp}^+$ is the Hama roughness function predicted by the i -th empirical model.

Figure 5 shows the maximum and average errors calculated from the ensemble predictions by NNTF, NN, and EMP. The predictions from NN exhibit 7.62% and 23.05% of average and maximum errors, respectively, while the predictions from NNTF exhibit 6.25% and 14.15% of the errors. Note that both NN and NNTF are performing better than EMP here. The most significant advantage of using transfer learning is in the reduction of the maximum error; nearly ten percentage of decrease is achieved by using NNTF instead of NN. This error reduction demonstrates the capability of NNTF in learning a better generalized mapping from a small amount of DNS data.

To further investigate the capability of transfer learning, the best and worst performing neural networks out of the 210 networks in NNTF and NN were pulled out and compared in figure 6. The errors from the best performing networks in NNTF and NN (figure 6a) show a similar trend as the ensemble predictions (figure 5); both average and maximum errors are significantly reduced by using transfer learning. It is also worth noting that the ensemble predictions from

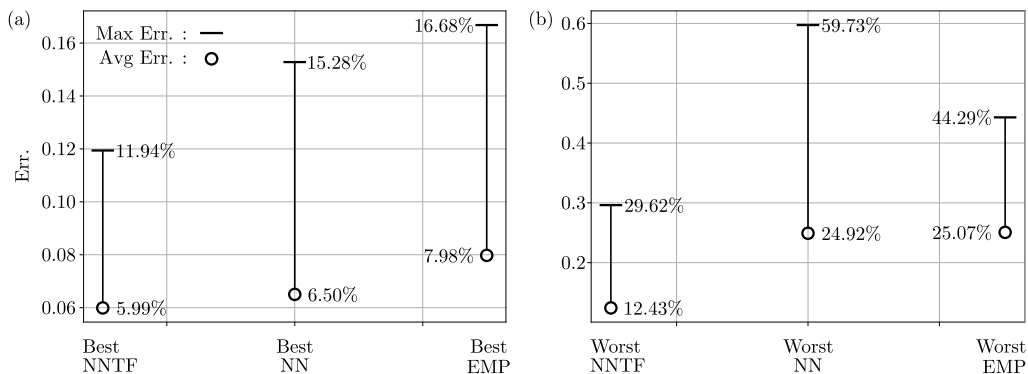


FIGURE 6. Average and maximum errors from the (a) best and (b) worst performing neural networks and empirical correlations.

NNTF (figure 5) perform better compared to both the best performing neural network in NN and empirical correlation in EMP (figure 6a).

The advantage of using transfer learning is more clearly demonstrated in the worst performing case (figure 6b). The maximum error of the worst performing neural network in NN is nearly 60%, showing that this network has failed to provide a reliable prediction. On the other hand, the network in NNTF exhibits significantly smaller errors, indicating that transfer learning is helping the network to provide a safer prediction even in the worst scenario. Therefore, these results show that transfer learning enables the networks to learn a more generalized mapping from limited DNS data by adapting an ‘approximate’ knowledge from empirical correlations. It is also important to emphasize that ensemble predictions should be used in practice to reduce the uncertainty arising from a limited pool of data as can be seen from the wide range of errors that occur with the best and worst performing neural networks in figure 6.

Finally, we investigate how transfer learning improves the generalization ability by characterizing the learning weights of the networks. Let w_l^i , where $l = 1, 2, \dots, N_w$, be the vectorized elements of the weight matrices $W_{j,k}^i$ in NN^i ($N_w = 488$ in this study). Then, we define the deviation of weights w_l^i from different NN^i as

$$\sigma_l = \frac{\sqrt{\sum_{i=1}^{210} (w_l^i - \mu_l)^2 / 210}}{\sum_{i=1}^{210} |w_l^i| / 210}, \quad (3.1)$$

where $\mu_l = \sum_{i=1}^{210} w_l^i / 210$. Note that the networks in NNTF were initialized with the pre-trained weights, and the networks in NN were initialized with the same random weights. Therefore, the deviation σ_l indicates how a weight in a neural network is updated differently for different combinations of training and validation data samples. In the ideal case with an infinite amount of data samples, the deviation will approach zero as the network would converge to specific weights representing an unique generalized mapping of the real physics.

The distributions of the deviation σ_l calculated from NNTF and NN are compared in figure 7. A number of weights with large σ_l are observed in NN, indicating that the updates of weights largely deviate depending on the data. This implies that the current data is insufficient for NN to learn a generalized mapping. On the other hand, the deviations are significantly reduced in NNTF, implying that the networks in NNTF are learning a better-generalized mapping compared to NN. This is because the networks in NNTF were initialized with the pre-trained weights containing the ‘approximate’ knowledge. These weights provide a better initial state for the weight optimization problem in the fine-tuning step.

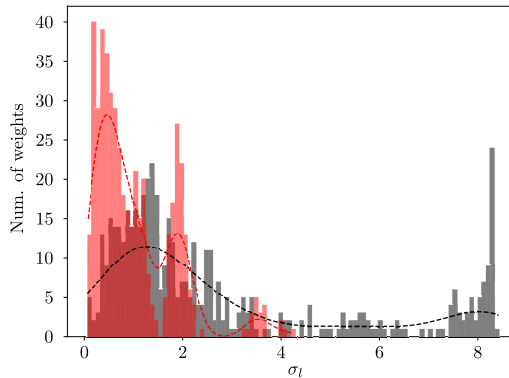


FIGURE 7. Distributions of the deviations of weights σ_l in NNTF (red) and NN (black).

4. Conclusion

We have developed a transfer learning framework to learn the Hama roughness function from a limited number of DNS data samples. The framework is composed of two steps: (1) pre-training step and (2) fine-tuning step. In the pre-training step, neural networks learn an ‘approximate’ knowledge from empirical correlations. In the fine-tuning step, the networks are fine-tuned using a small DNS dataset. Neural networks trained with transfer learning have shown a significant improvement in predicting the roughness function on test data samples not included in the fine-tuning step. This is because the pre-trained weights, containing the ‘approximate’ knowledge of empirical correlations, help networks to learn a better-generalized mapping of the real physics even from a small dataset. The developed framework can be applied to practical applications where only a limited amount of high-fidelity data is available. However, note that the networks would best perform on test data samples with similar origins of surfaces to those used in the fine-tuning step. Therefore, to further increase the generalization ability of neural networks, ultimately, the dataset has to be expanded. Accordingly, particular attention should be paid in the future to construct and train collective Big Data of flows over many types of rough surfaces in different flow conditions, such as the online [Roughness database](#) currently under construction.

Acknowledgements

This work was supported by the Swedish Energy Agency under Grant number 51554-1, Swedish Foundation for Strategic Research (FFL15-001), and Friedrich und Elisabeth Boysen-Foundation (BOY-151).

REFERENCES

- CHAKRABORTY, S. 2021 Transfer learning based multi-fidelity physics informed deep neural network. *Journal of Computational Physics* **426**, 109942.
- CHAN, L., MACDONALD, M., CHUNG, D., HUTCHINS, N. & OOI, A. 2015 A systematic investigation of roughness height and wavelength in turbulent pipe flow in the transitionally rough regime. *Journal of Fluid Mechanics* **771**, 743–777.
- CHEVALIER, M., LUNDBLADH, A. & HENNINGSON, D. S. 2007 Simson—a pseudo-spectral solver for incompressible boundary layer flow. *Tech. Rep.*
- CHUNG, D., CHAN, L., MACDONALD, M., HUTCHINS, N. & OOI, A. 2015 A fast direct numerical simulation method for characterising hydraulic roughness. *Journal of Fluid Mechanics* **773**, 418–431.
- CHUNG, D., HUTCHINS, N., SCHULTZ, M. P. & FLACK, K. A. 2021 Predicting the drag of rough surfaces. *Annual Review of Fluid Mechanics* **53**, 439–471.

- DALILI, N., EDRISSY, A. & CARRIVEAU, R. 2009 A review of surface engineering issues critical to wind turbine performance. *Renewable and Sustainable Energy Reviews* **13** (2), 428–438.
- FLACK, K. A. & SCHULTZ, M. P. 2010 Review of hydraulic roughness scales in the fully rough regime. *Journal of Fluids Engineering* **132** (4).
- FLACK, K. A., SCHULTZ, M. P. & BARROS, J. M. 2020 Skin friction measurements of systematically-varied roughness: Probing the role of roughness amplitude and skewness. *Flow, Turbulence and Combustion* **104** (2), 317–329.
- FOROOGHI, P., STROH, A., MAGAGNATO, F., JAKIRLIĆ, S. & FROHNAPFEL, B. 2017 Toward a universal roughness correlation. *Journal of Fluids Engineering* **139** (12).
- FUKAMI, K., FUKAGATA, K. & TAIRA, K. 2021 Machine-learning-based spatio-temporal super resolution reconstruction of turbulent flows. *Journal of Fluid Mechanics* **909**, A9.
- GENT, R. W., DART, N. P. & CANSDALE, J. T. 2000 Aircraft icing. *Philosophical Transactions of the Royal Society of London. Series A: Mathematical, Physical and Engineering Sciences* **358** (1776), 2873–2911.
- GOLDSTEIN, D., HANDLER, R. & SIROVICH, L. 1993 Modeling a no-slip flow boundary with an external force field. *Journal of Computational Physics* **105** (2), 354–366.
- HAMA, F. R. 1954 Boundary layer characteristics for smooth and rough surfaces. *Trans. Soc. Nav. Arch. Marine Engrs.* **62**, 333–358.
- JACOBS, T. D. B., JUNGE, T. & PASTEWKA, L. 2017 Quantitative characterization of surface topography using spectral analysis. *Surface Topography: Metrology and Properties* **5** (1), 013001.
- JOUYBARI, M. A., YUAN, J., BRERETON, G. J. & MURILLO, M. S. 2021 Data-driven prediction of the equivalent sand-grain height in rough-wall turbulent flows. *Journal of Fluid Mechanics* **912**, A8.
- KIM, J. & LEE, C. 2020 Prediction of turbulent heat transfer using convolutional neural networks. *Journal of Fluid Mechanics* **882**.
- KINGMA, D. P. & BA, J. 2014 Adam: A method for stochastic optimization. *arXiv preprint arXiv:1412.6980*.
- LEE, S. & YOU, D. 2019 Data-driven prediction of unsteady flow over a circular cylinder using deep learning. *Journal of Fluid Mechanics* **879**, 217–254.
- MOODY, L. F. 1944 Friction factors for pipe flow. *Trans. Asme* **66**, 671–684.
- PAN, S. J. & YANG, Q. 2009 A survey on transfer learning. *IEEE Transactions on Knowledge and Data Engineering* **22** (10), 1345–1359.
- PÉREZ-RÀFOLS, F. & ALMQVIST, A. 2019 Generating randomly rough surfaces with given height probability distribution and power spectrum. *Tribology International* **131**, 591–604.
- SCHULTZ, M. P., BENDICK, J. A., HOLM, E. R. & HERTEL, W. M. 2011 Economic impact of biofouling on a naval surface ship. *Biofouling* **27** (1), 87–98.
- YANG, J., STROH, A., CHUNG, D. & FOROOGHI, P. 2021 DNS-based characterization of pseudo-random roughness in minimal channels. *arXiv preprint arXiv:2106.08160*.